



ELSEVIER

Prototype studies of a fast RICH detector with a CsI photocathode

C. Lu^{a,*}, Z. Cheng^a, D.R. Marlow^a, K.T. McDonald^a, E.J. Prebys^a, I.H. Stairs^a,
R.L. Wixted^a, I. Adachi^b, R. Itoh^b, T. Sumiyoshi^b, N.S. Lockyer^c, J.E. Millan^c

^aJoseph Henry Laboratories, Princeton University, Princeton, NJ 08544, USA

^bKEK, National Laboratory for High Energy Physics, 1-1 Oho, Tsukuba-shi, Ibaraki 305, Japan

^cDepartment of Physics, David Rittenhouse Laboratories, University of Pennsylvania, Philadelphia, PA 19104, USA

Abstract

A prototype fast RICH detector with a CsI photocathode coupled to a wire chamber filled with atmospheric pressure ethane has been studied in a 3.5 GeV/c π^- beam. Using a 1 cm thick C_6F_{14} radiator, 8.5 photoelectrons per ring were detected. Measurements were made of the CsI quantum efficiency, photoelectron position resolution, and Cherenkov ring radius resolution. UV photon feedback appears to have degraded the resolution of the detector. Techniques to improve the photon detection efficiency and reduce backgrounds are discussed.

1. Introduction

In recent years there has been substantial effort in implementing the ring imaging Cherenkov detector (RICH) concept [1] using a solid CsI photocathode. We previously reported tests of a prototype RICH detector that observed Cherenkov rings with an average of five resolved photoelectrons using a 2 cm thick C_6F_{14} radiator [2]. Since then there has been significant progress in the systematic understanding of CsI photocathode preparation [3], so we have performed new studies of the prototype detector with an improved photocathode.

The prototype RICH detector is shown in Fig. 1. The CsI photocathode resides in a stainless steel chamber that contains a multiwire proportional chamber to amplify the Cherenkov photoelectrons. The Cherenkov light is produced in a 1 cm thick cell of liquid C_6F_{14} mounted just outside the UV grade quartz window of the chamber. The diameter of the anode wires is 20 μ m and their pitch is 2.54 mm. The gaps between the photocathode and the anode wire plane, and between the anode wire plane and the 80% transparent cathode mesh plane are both 5 mm. The distance between the quartz window and photocathode is 3.44 cm. The photocathode is subdivided into 348 photocathode pads, each 8×8 mm² in area and read out by one AMPLEX channel [4,5]. The beam tests were performed with 3.5 GeV/c pions at the KEK π^2 test beam in September 1994.

Section 2 discusses various measurements made on parameters of the prototype detector prior to the beam test. The setup for the beam test is reported in Section 3 and the

results of the test in Section 4. Conclusions and projections for future improvements are presented in Section 5.

2. Measurements of various prototype components

To be able to compare our beam test results with a reliable Monte Carlo calculation, we first measured the physical properties for various components of the prototype.

2.1. Photocathode substrate

Various groups have reported that the type and surface finish of the photocathode substrate can have a significant effect on quantum efficiency [6–8], presumably by influencing the size of the microcrystals of the deposited photocathode. This effect is not well understood at present, so we have begun studies into it. Here we make a preliminary report, and further details will be published elsewhere.

Our studies of photocathode substrates were conducted with a small test chamber consisting of a 7.5 cm diameter quartz window coated with a thin Cr film as anode, as aluminium plate as the photocathode substrate, and a G10 ring as a spacer between cathode and anode. We first evaporated a 1000 Å thick CsI photocathode on the aluminium plate and monitored its quantum efficiency with a vacuum monochromator and calibrated photomultiplier (described in Ref. [3]) for three days, during which there was no degradation.

We next replaced the aluminium plate with a Cu-clad G-10 plate and evaporated a 1000 Å thick layer of CsI on

* Corresponding author.

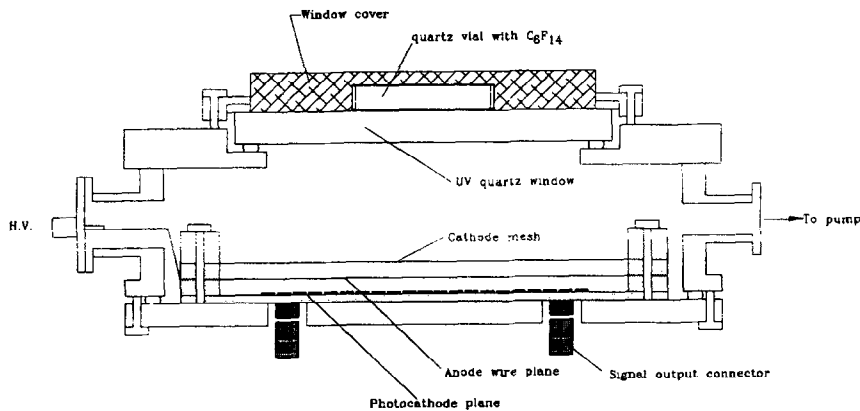


Fig. 1. Sketch of the fast RICH prototype.

the copper surface. The initial quantum efficiency of the CsI photocathode on the Cu-clad G-10 plate was only 80% of that on the aluminium plate, and a further 10% drop occurred over 2 days.

Then we cleaned the copper surface and evaporated 700 Å of aluminium onto it, followed by 1000 Å of CsI. The quantum efficiency of this photocathode was initially as good as that on aluminium plate, but after 3 days it dropped 10%.

These observations indicate that with an aluminium substrate we can get a high quantum efficiency, even when the aluminium is a thin layer deposited on a Cu-clad G-10 substrate, but in the latter case there may be some degradation during the first few days. In another set of observations we also confirmed that among Al, Au, Sn/Pb and Cu substrates Al is the one that supports the highest quantum efficiency of CsI [9].

We have also made a brief study of the effect of using a highly polished silicon wafer as the substrate. When CsI was deposited directly onto the silicon the quantum efficiency was no better than in the cases described above. However, when a 1000 Å layer of aluminium was first applied to the silicon, a very fresh 1000 Å thick CsI photocathode showed quite high quantum efficiency which stabilized after a few days to a representative value of 24% at 180 nm. This photocathode had the highest quantum efficiency of any in our tests and deserves further investigation.

On the basis of these studies, we evaporated a 650 Å thick aluminium film onto the gold-plated Cu-clad G-10 cathode plane of the prototype RICH detector prior to deposition of CsI.

2.2. Quantum efficiency of the photocathode

The CsI photocathode used for the beam test was 1170 Å thick. Its initial quantum efficiency was measured vs. wavelength with our vacuum monochromator with

results as shown in Fig. 2. We then sealed the prototype detector, transported it to KEK, Japan for the beam test, and brought it back to Princeton, where another measurement of the quantum efficiency was made with the vacuum monochromator. The time span between those two measurements was 15 days, over which there was no discernible degradation in the quantum efficiency. During this interval the chamber was pumped down to vacuum and repressurized with fresh gas at least every 2 days. Thus the quantum efficiency of the prototype detector was even more stable with time than the small test chamber with Al/Cu photocathode substrate discussed above.

The prototype chamber was evacuated and left sealed for 7 months following its return from KEK, during which the pressure rose to 20 Torr. Recently we pumped the chamber down, refilled it with ethane and measured the quantum efficiency to be 60% of its value 7 months earlier.

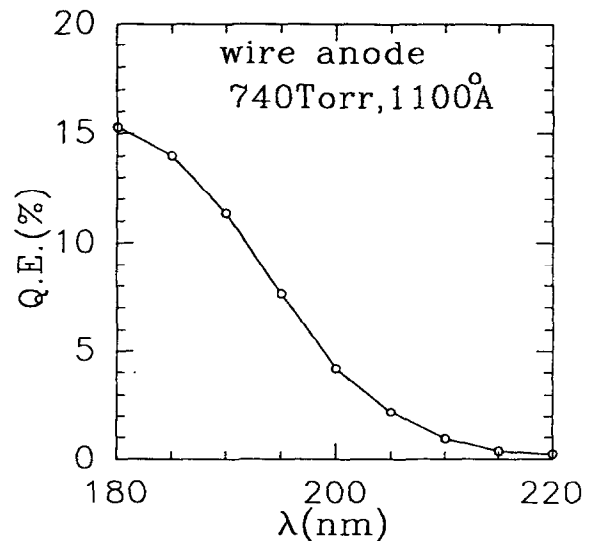


Fig. 2. Quantum efficiency of the photocathode.

2.3. Gas gain

The prototype RICH detector was operated with atmospheric pressure ethane. The gas gain with 740 Torr C_2H_6 was measured with an EG&G Ortec model 142PC pre-amplifier, model 570 amplifier and model 916 MCA system. The preamplifier was connected to one pad, and the UV beam from the VUV monochromator was positioned at the center of this pad. Due to charge sharing, the charge induced on one cathode pad across the 5 mm gap from the anode is $\sim 60\%$ of the charge on the cathode plane, and therefore 30% of the total signal charge on the anode. After this correction we determined the gas gain vs. high voltage; in particular, the beam test was performed at 4100 V in which the gas gain was 4.6×10^5 .

2.4. Transmittance of the liquid radiator

A 5 cm diameter, 1 cm thick UV quartz vial filled with purified C_6F_{14} liquid was used as a radiator. This vial was placed in our vacuum monochromator to measure its transmittance, and the C_6F_{14} was found to have excellent purity as delivered from the 3M Fluorinert Products Division. Passing the C_6F_{14} through Oxyorb produced no additional improvement in transparency. We did obtain some improvement by vacuum distillation. After 80% of the liquid was distilled we discarded the remaining 20%. This cycle was repeated several times, and then purified liquid was transferred to the quartz vial in a nitrogen-filled glove box. The transmittance of purified C_6F_{14} was then measured to be almost identical to that reported by the DELPHI Collaboration [10].

2.5. Transmittance of the quartz window

The 12.5 cm diameter, 1.27 cm thick UV quartz window was purchased from Wilmad Glass Co. We measured its UV transmittance and fit the results to the analytic form

$$T = 0.919 \exp(-1.275/0.000575(\lambda - 158.5)^{3.44}).$$

3. Beam test setup

The prototype RICH detector was tested at KEK in the π^2 test beam. The test beam layout is shown in Fig. 3. A 3.5 GeV/c π^- beam of typically 100 particles per 1 s spill was normally incident on the detector. A set of drift chambers tracked the beam particles. A gas Cherenkov

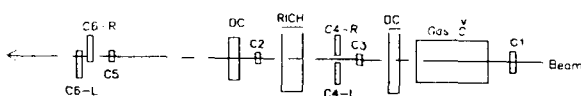


Fig. 3. Schematic layout of the test beam setup.

counter served to distinguish pions from electrons. Kaons were not distinguished from pions, but constituted less than 1% of the beam.

The readout electronics were based on AMPLEX VLSI chips [4,5]. Eight PC boards, each containing 3 AMPLEX chips and relevant control circuitry, are directly attached to the back side of the detector through 50-pin connectors. The control logic signals are issued by a LeCroy model 2366 Xilinx CAMAC module. Upon receipt of a system RESET signal from an output register and a TRIGGER signal from the trigger logic, the Xilinx module issues CLEAR and TRACK/HOLD signals, which are sent to all of eight boards through a daisy-chained flat cable. The Xilinx module also issues a series of CONVERT and CLOCK signals. The CLOCK signal is sent to the first card; subsequent cards receive the CLOCK-OUT signal from their predecessor. The CONVERT signal, after ECL/TTL conversion, is connected to the gate of custom CAMAC ADC module. Since the AMPLEX chip provides charge integration and pulse shaping (~ 750 ns), the latter plays a role as an analog delay line and there is no need for an additional delay cable.

In the university lab the electronics noise had a typical rms value of $\sigma \approx 1600 e^-$, but in the KEK test beam area the noise was doubled. As the detector was operated with a gas gain of 4.6×10^5 the signal induced on the photocathode pad plane by a single photoelectron was about 70 times the noise level.

4. Beam test results

4.1. Primary data analysis

Due to the relatively large gap between the anode and photocathode, the induced charge from an avalanche is distributed over several cathode pads. If two avalanches are close to each other and the corresponding groups of struck pads are merged. Because the drift distance from the center of the radiator of the photocathode was only 52 mm the probability of such overlap is not small.

To analyze the merged photoelectrons and reconstruct the Cherenkov rings, a simple pattern-recognition algorithm was employed as follows:

- Search for pads with charge at least 2σ above pedestal and ignore the remaining pads. The average photoelectron signal on the pad plane was 70σ , so pads sharing as little as $1/35$ of a single-photoelectron signal are kept.

- Group the nonzero pads into isolated clusters, each of which has a nonzero adjacent pads.

- Within each cluster search for peaks, and calculate the centroid and total charge for each peak. The charge on pads between multiple peaks is apportioned to each peak in the ratio of the charges in the pads containing the peaks.

- Merge two peaks into one if their centroids are separated less than 1.5 pad unit (1 pad unit = 8.1 mm). If

multiple peaks within a cluster are further apart than 1.5 pad unit, separate the cluster into resolved clusters.

– Retain those resolved clusters whose centroids satisfy $5.5 < r < 8.5$ pad units ($44 < r < 68$ mm), where r is the distance from the center of the Cherenkov ring as reconstructed by the drift-chamber tracking system. The accuracy of the latter system is $\sigma_x = \sigma_y = 0.2$ mm.

– Fit a circle (the Cherenkov ring) to the centroids of the resolved clusters that lie within the annulus defined above, using the reconstructed track position as the center.

4.2. Position resolution

In Fig. 4 the clusters from 5000 events are superimposed. Each point is the centroid of a resolved cluster found by the preceding algorithm. The (vertical) anode wires can be clearly seen in the figure. The very fine horizontal lines are due to small avalanches that induce charge on only one or two horizontally adjacent pads, or due to noise above the 2σ criterion. For such cases the vertical coordinate of the avalanche is taken as the center of the pad, leading to horizontal lines.

Fig. 4 also reveals that some electronics channels, especially in the upper right corner, were dead or not connected to their corresponding pads. The reconstructed centroids of clusters that induce charge on these dead pads are “pushed” away from the dead region by the charge-weighting algorithm.

We have previously studied the position resolution obtained using charge weighting of pads signals from single-photoelectron avalanches in the prototype chamber

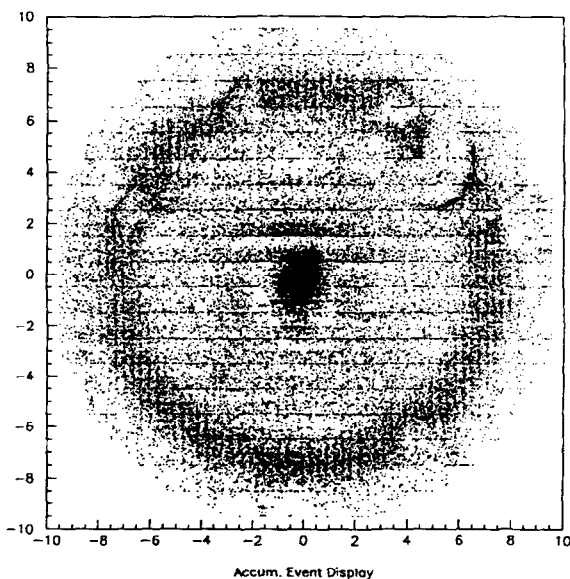


Fig. 4. Image of 5000 superimposed events to show the position resolution. Each point is the reconstructed x - y coordinate of a resolved cluster.

[3]. In the anode wire direction (vertical) $\sigma_y = 0.35$ mm has been archived, and in the perpendicular direction (horizontal) $\sigma_x = 2.54/\sqrt{12} = 0.73$ mm is obtained, where 2.54 is the anode wire pitch. In other words, we would be able to “see” the anode wires, as is the case in Fig. 4.

Fig. 5 shows the distribution of radii of all resolved clusters in the beam test data; the peak near $r = 7$ pad units is the Cherenkov ring and that near $r = 1$ is from ionization of the chamber gas by the beam particles. Clusters outside these two peaks are likely due to UV photon feedback. This effect has been noted in RICH systems that use TMAE vapor as the photosensitive element [10,11], and whose quantum efficiency spectrum is very similar to that of CsI.

The Cherenkov rings are reconstructed from the clusters with radii in the range $5.5 < r < 8.5$ pad units, as mentioned above. Fig. 6 shows the distribution of the best-fit radii of the reconstructed Cherenkov rings. In the fit we used the drift chamber track position as the center of the ring. The distribution is not well described by a single Gaussian; a double Gaussian is much more satisfactory. The parameters resulting from a double-Gaussian fit are average radius $\bar{r}_1 = 7.27$ pad units = 5.89 cm, $\sigma_{r_1} = 0.23$ pads = 0.186 cm and $\bar{r}_2 = 7.08$ pads, $\sigma_{r_2} = 0.42$ pads.

4.3. Yield of resolved clusters

The distribution of the number of resolved clusters per event within the annulus $5.5 < r < 8.5$ pad units is shown in Fig. 7. A Poisson distribution fits the data well. The mean number of resolved clusters is 7.1. This number is different from the true photoelectron yield due to cluster

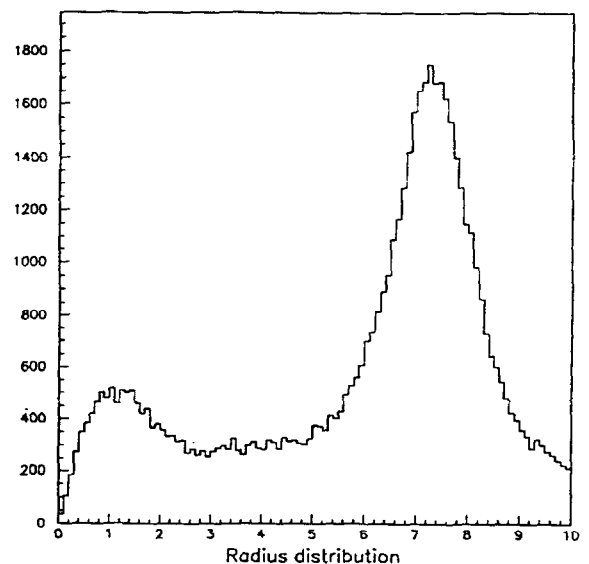


Fig. 5. Radial distribution in pad units (0.81 cm) of all resolved chambers in the beam test data.

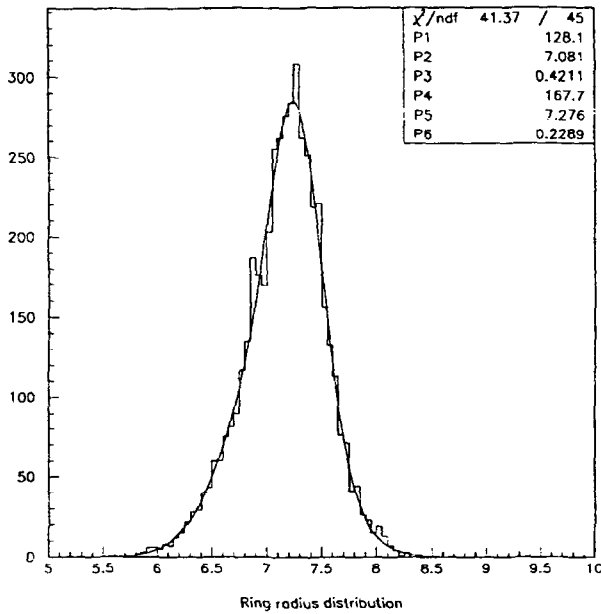


Fig. 6. The distribution of reconstructed Cherenkov-ring radii in pad units (0.81 cm).

overlap which reduces the apparent number of clusters, and due to UV photon feedback which increases the apparent number.

4.4. Monte Carlo simulation

To aid in further interpretation of the results from the beam test a Monte Carlo program has been written to

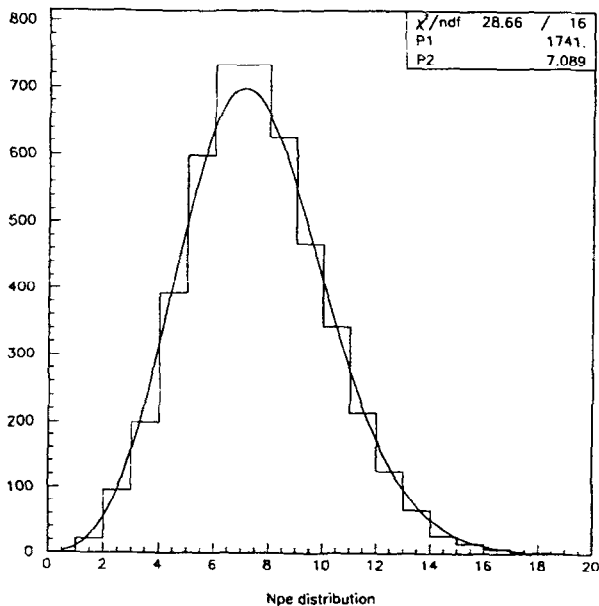


Fig. 7. Distribution of resolved clusters per event.

simulate the performance of the prototype RICH detector. All of the essential parameters and distributions, such as quantum efficiency of CsI photocathode, absorption length of C_6F_{14} and quartz window, gas gain and charge spectrum, were taken from the experimental measurements made away from the test beam as reported in Section 2. The simulation consisted of 2000 events for which induced-charge signals from Cherenkov photoelectrons were modelled according to charge sharing, and a simulated data file was generated. The same data analysis program was then run for the Monte Carlo generated data file as for the test beam data, and the main results are shown in Fig. 8.

The average number of Cherenkov photoelectrons produced in the Monte Carlo simulation is 9.5. Due to the overlap of induced-charge from the photoelectron avalanches, the number of clusters resolved by the cluster- and peak-finding algorithm is about 7.15, as shown in Fig. 8(d). The simulated distribution of Cherenkov-ring radii is well described by a single Gaussian with $\sigma_r = 0.134$ pad unit.

4.5. Background clusters

The beam test data (Fig. 4) show a substantial number of hits outside the annulus where Cherenkov hits are expected and away from $r=0$ where the beam particle ionizes the chamber gas. These background hits are, however, not uniformly distributed but appear to be associated with the Cherenkov ring and central beam spot, consistent with their being due to UV photon feedback.

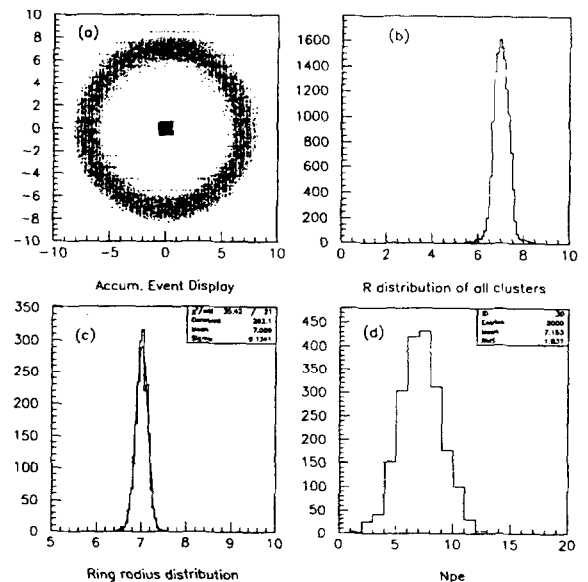


Fig. 8. Results of the Monte Carlo simulation without background. (a) Image of 2000 superimposed Monte Carlo events; (b) radial distribution of resolved clusters; (c) distribution fitted Cherenkov ring radii; (d) distribution of the number of resolved clusters per event. Spatial coordinates are in pad units (0.81 cm).

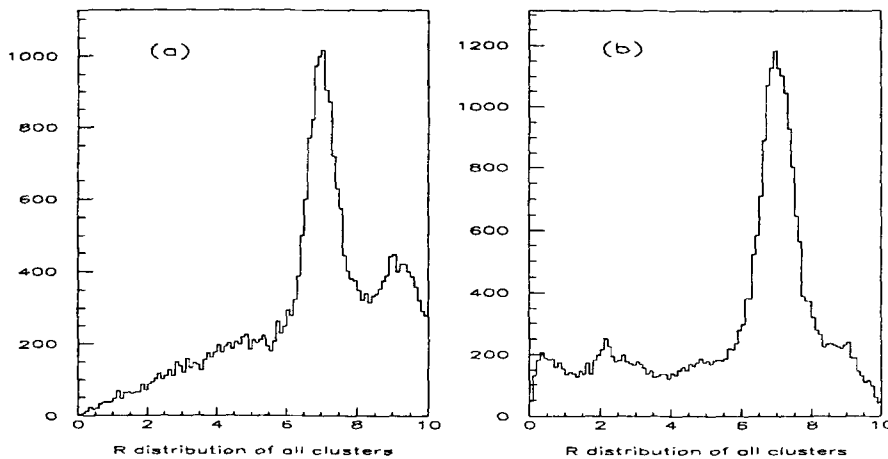


Fig. 9. The radial distribution of resolved clusters in a Monte Carlo simulation that includes avalanches from Cherenkov photoelectrons and background processes. (a) The background avalanches are uniformly distributed; (b) the background avalanches are due to UV photon feedback which is spatially correlated to Cherenkov photoelectrons. See text for details.

This hypothesis was further studied by a simulation of background hits. Fig. 9(a) shows the results of adding a spatially random distribution of hits to the simulation of the Cherenkov rings. The radial density of the background clusters varies linearly with increasing radius, in contrast to the beam test data. Fig. 9(b) shows a simulation modelled on UV photon feedback in which it is assumed that each photoelectron avalanche leads to two additional avalanches whose rms distance from the photoelectron is 2 pad units. The second background simulation is a much closer representation of the data, indicating the presence of photon feedback in the beam test data.

Feedback photon clusters are expected to cause a loss of accuracy in the reconstructed Cherenkov ring radius. The simulation with background clusters (Fig. 8(c)) shows a much narrower distribution of Cherenkov ring radii than does the beam test data (Fig. 6). The simulation that includes background clusters modelled on UV photon feedback (Fig. 9(b)) leads to a Cherenkov ring radius distribution with $\sigma_r = 0.213$ pad unit. This value is close to that of the narrower Gaussian of the double-Gaussian fit to Fig. 6, $\sigma_{r_1} = 0.23$ pad unit. However, the simulation does not reproduce the details of the double-Gaussian behavior observed in the test beam data. Further investigation is certainly needed.

4.6. Photoelectron yield

The number of resolved clusters in the beam test data in the vicinity of the Cherenkov ring, $5.5 < r < 8.6$ pad units, is 7.1. That radial band contains 96 pads of which 14 had electronics that were either dead or disconnected. We estimate that the fraction of lost clusters due to the dead channels was not 14/96 but only 1/10 because of charge sharing. That is, the corrected number of resolved clusters in the beam test data is 7.9.

The Monte Carlo simulation was used to relate the corrected number of resolved clusters to the number of Cherenkov photoelectrons per event. In the simulation the number of Cherenkov photoelectrons per event is $\bar{n} = 9.45$. Ignoring background, these photoelectrons lead to only $\bar{n} = 6.75$ resolved clusters in the simulation. The addition of two feedback photoelectrons for each Cherenkov photoelectron as discussed in Section 4.6 increases the number of resolved clusters to $\bar{n} = 8.72$ in the range $5.5 < r < 8.5$ pad units.

Hence the simulation indicates that the ratio of Cherenkov photoelectrons to resolved clusters is $9.45/8.72 = 1.08$. We then infer that the number of Cherenkov photoelectrons per event produced in the beam test was $7.9 \times 1.08 = 8.5$, which is 90% of that expected according to the simulation.

5. Conclusions and discussion

The principal conclusions from the beam test of the prototype RICH detector are:

- The yield of Cherenkov photoelectron was 8.5 per ring. This corresponds to 90% of the yield in a Monte Carlo simulation of the detector that includes the effect of UV photon feedback.

- The observed distribution of Cherenkov ring radius is better described by a double than single Gaussian. The narrower and larger Gaussian peak has $\sigma_r = 0.23$ pad unit, which is very close the value expected according to a Monte Carlo simulation. The broader Gaussian component is not yet understood in detail, but is likely related to UV photon feedback.

- Charge sharing among cathode pads results in very good position resolution for individual photoelectron avalanches; the anode wires can be clearly seen.

We anticipate that the performance of the RICH detector can be improved in several ways. Indeed, Almeida et al. recently demonstrated a prototype RICH detector that produced 14 photoelectrons per Cherenkov ring with a CsI cathode whose quantum efficiency was not larger than ours [12]. Possible improvements to our detector include:

1) Use of highly polished photocathode substrates. Our best preliminary result (Section 2.1) indicates that we might obtain a CsI quantum efficiency 1.5 times that of the beam test.

2) Use of a cathode mesh of greater transparency. In the present detector the cathode mesh on the entrance side of the chamber gap was 80% transparent to normally incident light, corresponding to only 70% transmission of light at the Cherenkov angle. A factor of 1.15 improvement would be obtained by use of 90% transparent mesh. Essentially all loss of light to the mesh could be avoided by coating it with CsI; a brief test of this concept for the prototype detector coupled to the vacuum monochromator showed a factor of 1.2 improvement.

3) The number of resolved clusters can be increased by increasing the distance between the C_6F_{14} radiator and the photocathode and hence increasing the separation between photoelectrons. This distance was only 5.2 cm in our prototype, much smaller than the ≈ 20 cm that would be appropriate in the final design.

4) The number of resolved clusters would also be increased by decreasing the gap between the anode and the cathode. Our prototype used 5 mm for this gap to improve the position resolution for individual photoelectrons via charge sharing on the cathode pads. However, this also increased the probability that nearby avalanches would lead to merged clusters.

5) The background due to UV photon feedback can be reduced by adding isobutane to the chamber gas. Avalan-

ches of hydrocarbon gases lead to UV photons with energy 10.2 eV from de-excitation of hydrogen (Lyman- α) and energies 7.94, 7.48 and 6.43 eV from de-excitation of carbon [10]. Ethane is transparent to the 6.43 and 7.48 eV photons, and largely so to the 7.94 eV photon. Isobutane is only transparent to the 6.43 eV photon. Since a quartz window has similar UV absorption to isobutane there is little additional loss of Cherenkov photons is adding isobutane to a chamber with a quartz window.

Together the proposed improvements offer the prospect of a factor of 1.8 increase in photoelectron yield and much lower backgrounds due to photon feedback. The resulting detector would have performance of the quality needed for large-scale use in particle identification systems for high-energy-physics experiments.

References

- [1] J. Séguinot and T. Ypsilantis, Nucl. Instr. and Meth. 142 (1977) 377.
- [2] N.S. Lockyer et al., Nucl. Instr. and Meth. A 332 (1993) 142.
- [3] C. Lu et al., Princeton/HEP/94-10 (June 12, 1994), submitted for publication in Nucl. Instr. and Meth.
- [4] E. Beuville et al., Nucl. Instr. and Meth. A 288 (1990) 157.
- [5] R. Wixted, Princeton U. Internal Report (28 March, 1994).
- [6] D.F. Anderson, S. Kwan and V. Peskov, Nucl. Instr. and Meth. A 343 (1994) 109.
- [7] P. Križan et al., IJS Report IJS-DP-7087 (October 1994), submitted for publication in Nucl. Instr. and Meth.
- [8] J. Almeida et al., WIS-95/14/March-PH (March 95).
- [9] W. Kononenko, private communication.
- [10] R. Arnold et al., Nucl. Instr. and Meth. A 270 (1988) 255.
- [11] D. Leith, Nucl. Instr. and Meth. A 265 (1988) 120.
- [12] J. Almeida et al., Nucl. Instr. and Meth. 367 (1995).